A hybrid PSTD/DG method to solve the linearized Euler equations

Raúl Pagán Muñoz and Maarten Hornikx
Department of the Built Environment, Eindhoven University of Technology, Eindhoven, The Netherlands.

Summary
The Fourier Pseudospectral Time Domain (Fourier-PSTD) method was shown to be an effective way of modelling wave propagation. Fourier-PSTD is based on Fourier analysis and synthesis to compute the spatial derivatives of the governing wave equation. Therefore, the method suffers from the well-known Gibbs phenomenon when computing a non-smooth or discontinuous function. This limits its possibilities to compute arbitrary boundary conditions. Furthermore, the method needs to be computed on a regular mesh. Although some developments have been presented to locally refine the grid using multidomain implementations, its performance is limited when computing complex geometries. This paper presents a hybrid approach to solve the linearized Euler equations, coupling the Fourier-PSTD method with a nodal Discontinuous Galerkin (DG) method. DG exhibits almost no restrictions with respect to geometrical complexity or boundary conditions. The aim of this novel method is to allow the computation of arbitrary boundary conditions and complex geometries by using the benefits of the DG method while keeping Fourier-PSTD in the bulk of the domain. In this paper, a coupling algorithm is presented together with an analysis of the precision of the hybrid approach.

PACS no. 43.28.Js

1. Introduction

In general, accurate solutions and long time integrations are sought when computing sound propagation. Optimization of the computational resources is needed in addition to the precision and stability of numerical methods, which remains challenging in computational acoustics community. In this sense, the benefits of using high order methods when solving time dependent problems have already been documented, for instance, by Hesthaven et al. [1]. Among high order methods, Fourier pseudospectral techniques have shown to be an effective way of modelling sound propagation, e.g., [2]. These methods use all the information available in the domain to compute the spatial derivatives. In contrast, the well-known and widely used finite-differences time domain (FDTD) method [3] uses local information around the point where the derivative is calculated. The Fourier Pseudospectral Time Domain (Fourier-PSTD) method belongs to the family of Fourier spectral techniques. Both methods, FDTD and Fourier-PSTD, discretize the physical domain in a regular mesh, calculating the solutions at discrete points. In Fourier-PSTD, the spatial variables are transformed through a set of basis functions and the derivatives are computed in the transformed domain. Since the chosen basis functions consist of (periodic) trigonometric polynomials, the domain transformation can be computed by fast Fourier transforms (FFT). The main benefit is that Fourier-PSTD requires only the theoretical minimum number of points (two per wavelength) to solve the acoustic problem of interest with spectral accuracy, as shown by Liu [4]. Therefore, Fourier-PSTD is based on Fourier analysis and synthesis to compute the spatial derivatives of the governing equation while the time-marching scheme is operated by another method, e.g., Runge-Kutta (RK). Fourier-PSTD is an efficient algorithm to calculate sound propagation but it suffers from the well-known Gibbs phenomenon when computing the derivatives of a non-smooth or discontinuous function. This major limitation, caused by the periodicity assumed in the FFT, can be solved, e.g., by using perfectly match layers (PML) [5]. Treatment of rigid boundaries and boundaries with a different density have successfully been presented [2], and an approximation for impedance boundary conditions has been made [6]. However, no accurate solution to impedance boundary conditions has been presented thus far. Furthermore, as mentioned, the

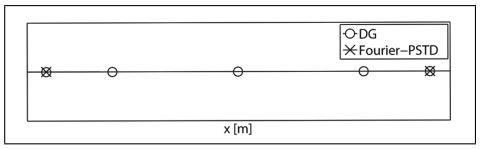

Figure 1: Hybrid overlapping mesh with $m_{hyb} = 1$ and $N_{DG} = 4$ (one Fourier-PSTD and one DG element).

method needs to be computed on a regular mesh. Although, some developments have been presented by Hornikx et al. [7] to locally refine the grid using multidomain implementations, its performance is limited when computing complex geometries.

The idea of coupling methodologies in order to get the benefits of each solver has already been presented, for instance, by Utzmann et al. [8]. With the purpose of including arbitrary boundary shapes and conditions in the Fourier-PSTD method, this paper presents a hybrid approach to solve the linearized Euler equations (LEE), coupling Fourier-PSTD with a nodal Discontinuous Galerkin time domain (DG) method [9]. DG is a finite element scheme that operates in a functional space of piecewise polynomial functions with no continuity constraint at cell interfaces. The cells are connected to its neighbours via numerical flux terms based on the values of the solutions at both sides of the interface. The method computes the spatial derivatives of the governing equations using a variational formulation while the time-dependent part of the equation can be computed using, e.g., a low-storage RK scheme [10] [11]. Therefore, DG is a local method that exhibits almost no restrictions with respect to geometrical complexity, it allows to locally refine the polynomial order and/or the element size, and it is well suited for parallel computing. Furthermore, boundary impedance condition formulations already exist, e.g. [12]. On the other hand, DG does not achieve the power resolution of Fourier-PSTD, what limits the efficiency of the hybrid method respect the standalone Fourier-PSTD solver. Moreover, in this paper, the nodes within the DG elements are the Legendre-Gauss-Lobatto (LGL) non-equally spaced quadrature points (see figure 1), while Fourier-PSTD works on orthogonal equidistant grids. Therefore, the hybrid methodology needs to include spatial interpolation to reconstruct the values everywhere. Finally, the Courant-Friedrichs-Lewy (CFL) condition, limiting the time stability of the methods, is more restrictive in DG than in Fourier-PSTD when solving the same scenario. Hence, the time steps in both solvers will be different and the data exchange between them will only be done at Fourier-PSTD time steps.

In this paper, a coupling algorithm between Fourier-PSTD and DG is presented to solve the LEE for a one dimensional case. The aim of this novel method is to allow the computation of arbitrary boundary conditions and complex geometries by using the benefits of DG while keeping Fourier-PSTD in the bulk of the domain. Section 2 includes a description of the physical model and the standalone solvers. Section 3 focuses on the hybrid technique while an analysis of its precision is presented in section 4.

2. Physical model and numerical methods

The main features of the physical model and the numerical methods are presented in this section. From now on, all the common variables will be indicated with the subscript PS or DG when they refer to Fourier-PSTD or to nodal DG time domain method, respectively.

2.1. Physical model

The physical model investigated in this paper is governed by the LEE for the solution of acoustic propagation problems. To simplify the model, the propagation medium is at rest and its temperature is constant in space and time. In three-dimensional (3D) Cartesian coordinates, the governing equation 1 in non-conservative form reads:

$$\frac{\partial \mathbf{q}}{\partial t} + \mathbf{A_j}\frac{\partial \mathbf{q}}{\partial j} + \mathbf{C}\mathbf{q} = 0, \tag{1}$$

$$\mathbf{A_j} = \begin{bmatrix} u_{0,j} & \rho_0\delta_{x,j} & \rho_0\delta_{y,j} & \rho_0\delta_{z,j} & 0 \\ 0 & u_{0,j} & 0 & 0 & \frac{\delta_{x,j}}{\rho_0} \\ 0 & 0 & u_{0,j} & 0 & \frac{\delta_{y,j}}{\rho_0} \\ 0 & 0 & 0 & u_{0,j} & \frac{\delta_{z,j}}{\rho_0} \\ 0 & \gamma p_0\delta_{x,j} & \gamma p_0\delta_{y,j} & \gamma p_0\delta_{z,j} & u_{0,j} \end{bmatrix}$$

$$\mathbf{C} = \begin{bmatrix} \frac{\partial u_{0,j}}{\partial j} & \frac{\partial \rho_0}{\partial x} & \frac{\partial \rho_0}{\partial y} & \frac{\partial \rho_0}{\partial z} & 0 \\ \frac{u_{0,j}}{\rho_0}\frac{\partial u_{0,x}}{\partial j} & \frac{\partial u_{0,x}}{\partial x} + D & \frac{\partial u_{0,x}}{\partial y} & \frac{\partial u_{0,x}}{\partial z} & 0 \\ \frac{u_{0,j}}{\rho_0}\frac{\partial u_{0,y}}{\partial j} & \frac{\partial u_{0,y}}{\partial x} & \frac{\partial u_{0,y}}{\partial y} + D & \frac{\partial u_{0,y}}{\partial z} & 0 \\ \frac{u_{0,j}}{\rho_0}\frac{\partial u_{0,z}}{\partial j} & \frac{\partial u_{0,z}}{\partial x} & \frac{\partial u_{0,z}}{\partial y} & \frac{\partial u_{0,z}}{\partial z} + D & 0 \\ 0 & \frac{\partial p_0}{\partial x} & \frac{\partial p_0}{\partial y} & \frac{\partial p_0}{\partial z} & \gamma\frac{\partial u_{0,j}}{\partial j} \end{bmatrix}$$

$$\mathbf{D} = \frac{\partial u_{0,j}}{\partial j} + \frac{u_{0,j}}{\rho_0}\frac{\partial \rho_0}{\partial j}$$

the acoustic variables $\mathbf{q} = [\rho, u_x, u_y, u_z, p]^T$ are ρ the density, u_j the velocity components with index j equals to x, y or z, and p the pressure. γ is the heat capacity ratio and δ denotes the Kronecker delta function. The sound speed can be calculated as $c^2 = \gamma p_0/\rho_0$. The physical variables are decomposed into their ambient values, denoted by subscript 0, and the acoustic fluctuations. Since the propagation medium is at rest in this work, the ambient velocity $u_{0,j}$ is equal zero as well as matrix $\mathbf{C}$. The viscous effects are neglected in the equations. The set is completed with initial and boundary conditions.

2.2. Fourier-PSTD method

Fourier-PSTD is a global wave-based time-domain method suitable for the computation of acoustic propagation problems governed by equation 1. The method is computed in a regular mesh and the grid spacing is determined by the smallest wavelength of interest. The gradients are calculated in the wavenumber domain using equation 2, by multiplying the transformed variables times ik_j, with i the imaginary number and k_j the wavenumber vector in Cartesian direction j, as shown in equation 3. The transformation of the discrete acoustic variables is done by using Fourier analysis and synthesis ($\mathcal{F}$ and $\mathcal{F}^{-1}$ are the forward and inverse Fourier transform, respectively).

$$\frac{\partial \mathbf{q}}{\partial j} = \mathcal{F}^{-1}(ik_j \mathcal{F}(\mathbf{q})) \tag{2}$$

$$k_j = \frac{2\pi n_{j,PS}}{N_{j,PS}\Delta r_{j,PS}} \tag{3}$$

with $n_{j,PS} \in [-\frac{N_{j,PS}}{2}+1, -\frac{N_{j,PS}}{2}+2, ..., \frac{N_{j,PS}}{2}]$, $N_{j,PS}$ the total number of grid points in the Cartesian direction j and $\Delta r_{j,PS}$ the equidistant grid spacing in that direction.

2.3. Nodal DG time domain method

DG divides the computational domain into B_{DG} non-overlapping conforming elements. The nodal DG scheme approximates the acoustic variables in the computational domain by a direct sum of B_{DG} local polynomials ($\mathbf{q^b}$) of order N_{DG}, and $N_{b,DG}$ is the number of nodal LGL quadrature points in each DG element. The boundary of each element b is indicated as ∂b. In this work, the DG time domain method computes the solution of the LEE using nodal Jacobi polynomials.

The semi-discrete formulation of the LEE, following the work by Toulorge et al. [11] and Reymen et al. [13] is shown in equation 4:

$$\mathbf{M}^b \frac{\partial \mathbf{q}^b}{\partial t} - \sum_{r=1}^{D_{DG}} \mathbf{K}_r^b \mathbf{A}_r^b \mathbf{q}^b + \cdots \cdots + \sum_{i=1}^{F_{DG}} \mathbf{M}^{\partial b_i} \hat{\mathbf{f}}^{\partial b_i} + \mathbf{M}^b \mathbf{C}^b \mathbf{q}^b = 0 \tag{4}$$

where $\mathbf{M}$ and $\mathbf{K}$ represent the mass and stiffness matrices, respectively, $\mathbf{A}$ and $\mathbf{C}$ are defined in section 2.1 and $\hat{\mathbf{f}}^{\partial b}$ is the numerical flux. Finally, index D_{DG} represents the dimensionality of the problem and F_{DG} the number of faces of each DG element. The numerical flux depends only on two values q_h^- and q_h^+ on elements b^- and b^+ that share ∂b. For this work, a fully upwind flux scheme has been chosen that has optimal dissipation properties when solving linear PDE's.

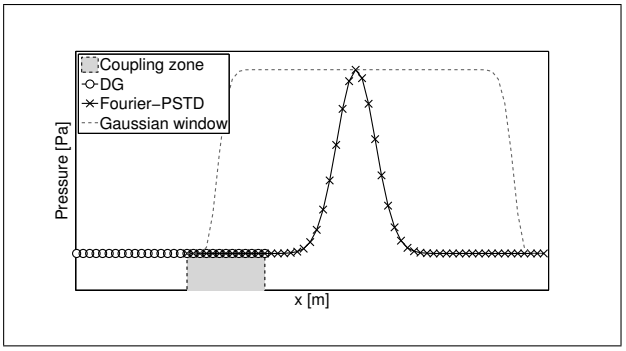

Figure 2: Initial pressure distribution in the 1D hybrid domain and detail of the Gaussian window. The CZ is indicated in the figure where both meshes overlap.

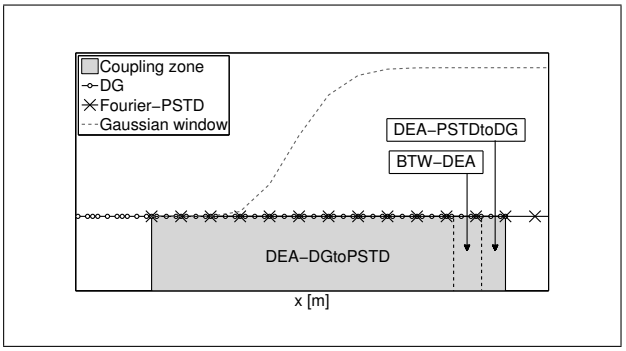

Figure 3: The three areas of the CZ: data-exchange area from Fourier-PSTD to DG (DEA-PStoDG), data-exchange area from DG to Fourier-PSTD (DEA-DGtoPS) and area between them (BTW-DEA).

2.4. Time integration scheme

The time derivatives of the governing equationS are computed in both solvers using low-storage Runge-Kutta schemes. Fourier-PSTD is calculated using the optimized six-stage RK method presented by Bogey and Bailly [14], referred as RKo6s; while for DG, the performance of three different RK schemes are compared in this work: RKo6s, the forth-order five-stage scheme presented by Carpenter [15] (RK54) and the optimized forth-order eight-stage scheme (RKF84) derived by Toulorge and Desmet [11].

3. Hybrid methodology

The 1D hybridization method presented in this paper is based on structured meshes for both solvers, where the size of the DG elements is forced to be an integer number of the size of the Fourier-PSTD elements as shown in figure 1 ($\Delta r_{DG} = m_{hyb}\Delta r_{PS}$ where, $m_{hyb} \in \mathbb{N}_1$. The index j in the variables is omitted for the 1D case) and the size Δr_{PS} is determined by the smallest wavelength of interest. In

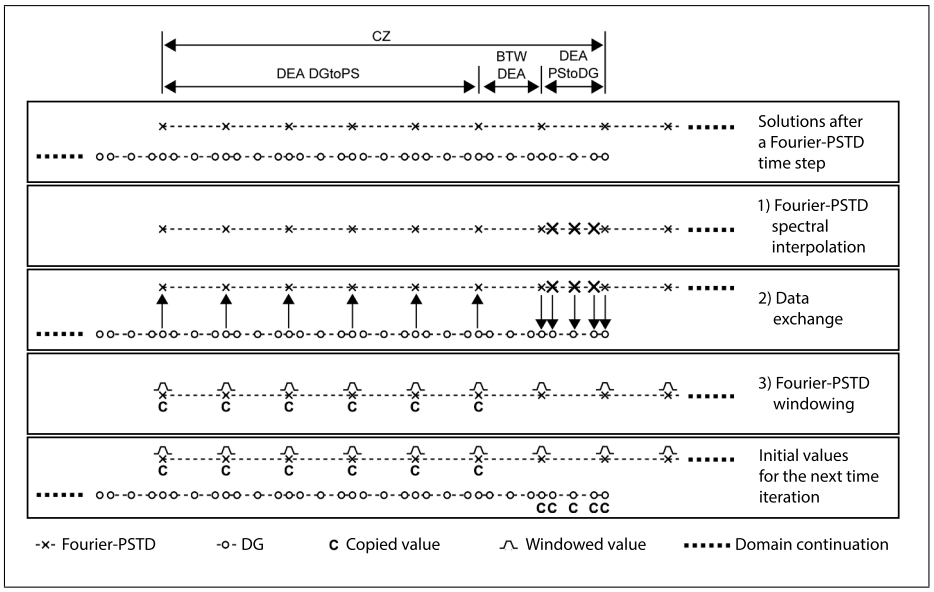

Figure 4: Post-processing and data exchange in the coupling zone ($m_{hyb} = 1$ and $N_{DG} = 4$)

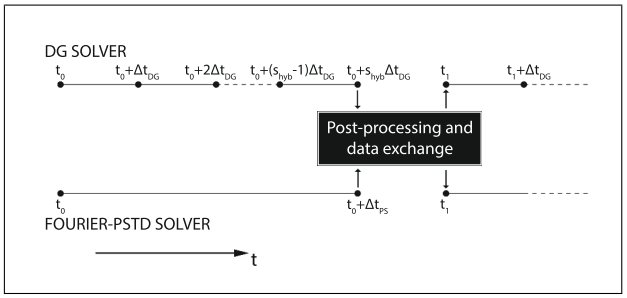

Figure 5: Time diagram of the hybridization process.

this work, only the case where $m_{hyb} = 1$ is investigated, where the Fourier-PSTD nodes are coincident with some of the DG nodes. Therefore, no spatial interpolation is needed before copying values from DG to Fourier-PSTD. The computational domain is spatially divided into a Fourier-PSTD subdomain and a DG subdomain with a coupling zone area (CZ) as illustrated in figure 2. The CZ is the data-exchange area between solvers where both meshes overlap and have some coincident nodes. The CZ is divided in a data-exchange area from Fourier-PSTD to DG (DEA-PStoDG), a data-exchange area from DG to Fourier-PSTD (DEA-DGtoPS) and a third area between them (BTW-DEA), as illustrated in figures 3 and 4. The maximum frequency ($f_{max,PS}$), limited by the spatial Nyquist condition in Fourier-PSTD, corresponds to a grid spacing $\Delta r_{PS} = c/(2f_{max,PS})$ or two points per wavelength. In this work, the results are limited up to $f_{max,hyb} = c/(2.5\Delta r_{PS})$.

3.1. Initial and boundary conditions

The initial conditions imposed in Fourier-PSTD are a broadband pressure and velocity distribution $p(x,t_0) = e^{-b_s(x-x_s)^2}$, $u(x,t_0) = -p(x,t_0)/\rho_0 c$, where b_s determines the bandwidth of the spectrum and x_s the source location. In this work, $b_s = 1/(2(2.5\Delta r_{PS})^2)[m^{-2}]$ is used. Figure 2 is showing the initial pressure distribution in the 1D hybrid domain. In DG, the time domain computation is initialized with a zero-valued pressure and velocity distribution. Relative to the boundary conditions, a window to obtain periodicity is used in Fourier-PSTD (see section 3.4). While for DG, the left end of the domain is computed using an acoustically rigid boundary while the right end is where the values from Fourier-PSTD are copied.

3.2. Time iteration, post-processing and data exchange

The hybrid time process is schematically shown in figure 5. The data is post-processed and exchanged after every Fourier-PSTD time step, Δt_{PS}. The three steps taken in the post-processing and data exchange process are shown in figure 4. Step 1) consists of the spectral-interpolation of the Fourier-PSTD solution in order to find the values at the DG nodes in the DEA-PStoDG area. In step 2), data is exchanged between solvers in the data-exchange areas. Finally, to obtain spatial periodicity and avoid Gibbs phenomenon, the acoustic Fourier-PSTD variables are multiplied by a Gaussian window in step 3) before computing the next time step.

In Fourier-PSTD, the time step is chosen to be $\Delta t_{PS} = CFL_{PS}\Delta r_{PS}/c$ while, DG time step is calculated from the expression $\Delta t_{DG} = \Delta t_{PS}/s_{hyb}$ where, $s_{hyb} \in \mathbb{N}_1$. Therefore, the Fourier-PSTD time step is an integer number of DG time steps. In this work, $CFL_{PS} = 0.5$ is used, while the hybrid method is investigated for different values of s_{hyb}.

3.3. Spectral interpolation

Spectral interpolation is computed for each non-coincident DG node g with coordinates $x_{g,DG}$ in the DEA-PStoDG area. The value at each DG node is interpolated from the closest Fourier-PSTD node, with $\Delta x_{g,int}$ the distance between them. The values of the variables at each missing DG location are computed in the wavenumber domain by using equation 5.

$$\mathbf{q_{g,int}} = \mathcal{F}^{-1}(e^{-ik\Delta x_{g,int}}\mathcal{F}(\mathbf{q})) \tag{5}$$

3.4. Fourier-PSTD Gaussian window

The field Fourier-PSTD variables are multiplied by a Gaussian window to obtain periodicity. The Gaussian window acts like a PML at the boundaries of the Fourier-PSTD domain. The single side exponential part of the window has $N_{w,PS}$ number of points and it is coincident with the DEA-DGtoPS area. The total number of points of the window is equal to the total number of Fourier-PSTD nodes, N_{PS}. The main parameters of the Gaussian window, i.e $N_{w,PS}$, α_w and β_w, are selected following the indications in [7].

4. Analysis of the hybrid methodology

To find an optimum implementation of the hybrid methodology, it is needed to determine and quantify the sources of error in order to select a suitable combination of parameters. Along this section, the error is quantified by comparing the transformed acoustic variables from the numerical methods with the analytical solutions using equations 6 and 7.

$$\epsilon_{amp}(f_i) = 20log_{10}\left|\left(\frac{|Q_a(f_i)| - |Q_h(f_i)|}{|Q_a(f_i)|}\right)\right| \tag{6}$$

$$\epsilon_{pha}(f_i) = 20log_{10}\left(\frac{|\phi[Q_a(f_i)] - \phi[Q_h(f_i)]|}{\pi}\right) \tag{7}$$

where, Q_a and Q_h are the analytical and numerical method solutions, respectively. Both are computed from the transformation of the time recorded variables to the frequency domain. Both errors will be expressed as the maximum error in the frequency range $[0, f_{max,hyb}]$, $\epsilon_{amp,max}$ and $\epsilon_{pha,max}$. The errors in this work are computed from the sound pressure solutions.

Unless otherwise indicated, these are the main parameters used in this work: 1) the results are presented up to $f_{max,hyb} = 12000$ [Hz]; 2) the corresponding spatial discretization is $\Delta r_{PS} = \Delta r_{DG} = 0.011$ [m]; 3) the sizes of the different areas are [DEA-PStoDG, BTW-DEA, DEA-DGtoPS]=[1,1,100] elements; 4) the limits of the hybrid domain are $[x_{min,hyb}, x_{max,hyb}] = [-1.178, 5]$ [m] and the right limit of the DG domain is always located at $x_{max,DG} = 0$ [m]; 5) the excitation is located at $x_s = 0.5$ [m] and the recording position at $x_{rec} = 2$ [m]; 6) the pressure is recorded up to $t_{rec} = 4247\Delta t_{PS}$ [s]; and 7) the parameters of the Gaussian window are $N_{w,PS} = 100$, $\alpha_w \simeq 7.4$ and $\beta_w = 3$.

Table I: RK scheme comparison for the DG solver and DG polynomial order and time step optimization.

	RKo6s	RK54	RKF84
$[N_{DG}, s_{hyb}]_{\epsilon_{amp}}$	[5,5]	[5,8]	[5,3]
$[N_{DG}, s_{hyb}]_{\epsilon_{pha}}$	[4,8]	[4,5]	[4,3]

Table II: Hybrid method amplitude and phase maximum errors compare with Fourier-PSTD and DG standalone solvers.

	Hybrid	Fourier-PSTD	DG
$\epsilon_{amp,max}$ [dB]	-47.6	-48.0	-63.7
$\epsilon_{pha,max}$ [dB]	-27.0	-27.0	-55.7

4.1. DG RK scheme and parameter study

The method has been evaluated and optimized for different RK time schemes in the DG solver: RK06s, RK54 and RKF84, while keeping RKo6s for the Fourier-PSTD computations. For each of them, all combinations of $3 \leqslant N_{DG} \leqslant 10$ and $1 \leqslant s_{hyb} \leqslant 10$ have been computed in order to find the optimum stable cases. The lowest values of the combination $[N_{DG}, s_{hyb}]$ that give a convergent solution are presented in table I. The convergence of the solution is evaluated by comparing $\epsilon_{amp,max}$ and $\epsilon_{pha,max}$ for each case with the smallest values of the errors of all stable combinations. The results show that all RK schemes give optimum results for polynomial order $N_{DG} = 5$. But, while RKo6s and RK54 require 5 and 8 DG time steps, respectively, to get a convergent stable solution, RKF84 requires only 3. Clearly, the optimum case is achieved with RKF84 scheme, though, it needs more RK stages.

4.2. Hybrid method precision

The precision of the hybrid method is evaluated for the optimum scenario found in section 4.1. The errors are compared with the Fourier-PSTD and DG standalone solutions when computing the same case. The results in figure 6 show that ϵ_{amp} and ϵ_{pha} of the hybrid method and the Fourier-PSTD standalone solver almost collapse in the graphs. The difference of the maximum amplitude errors between both methods is about 0.4 dB, while no difference is found for the maximum phase error, as shown in table II.

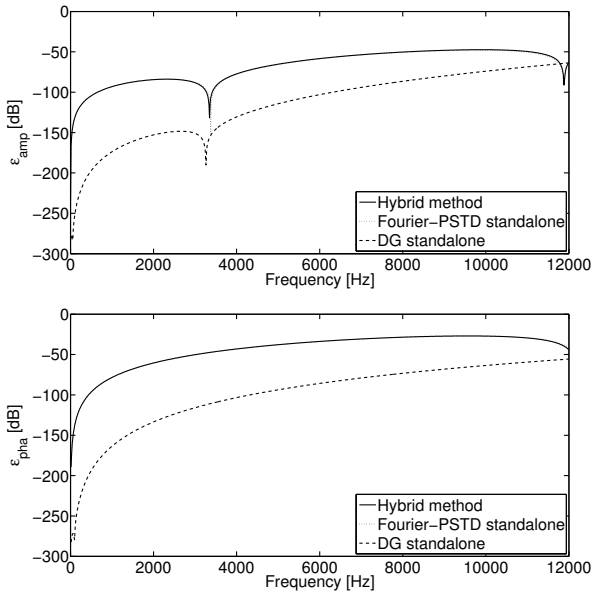

Figure 6: ϵ_{amp} and ϵ_{pha} of the hybrid method compare with the standalone solvers (hybrid and Fourier-PSTD standalone errors almost collapse).

5. CONCLUSIONS

A hybrid methodology has been presented to solve the LEE. The approach is suitable for computing boundaries using the benefits of DG while keeping Fourier-PSTD in the bulk of the domain. The method couples the regular mesh of Fourier-PSTD with the non-equally spaced DG nodes. In this work, both grids are conformed to avoid spatial interpolation of the DG variables, while, spectral interpolation of the Fourier-PSTD solution is still needed. During the hybridization process, the data is exchanged between solvers every Fourier-PSTD time step. Moreover, a Gaussian window is used to obtain periodicity in the Fourier-PSTD domain.

The hybrid methodology has been evaluated for different RK time schemes. The best performance for the evaluated scenario is achieved when using RKF84 in the DG solver and the parameters $N_{DG} = 5$ and $s_{hyb} = 3$ ($CFL_{DG} = 1$). The error of the novel methodology is almost identical to the error of the Fourier-PSTD standalone solver up to 2.5 points per wavelength for the evaluated example. This latter conclusion motivates to keep developing the method towards higher dimensions. Current work is directed towards optimizing the lengths of the areas of the coupling zone as well as the Gaussian window parameters.

Acknowledgement

The research leading to these results has received funding from the People Programme (Marie Curie Actions) of the European Union's Seventh Framework Programme FP7/2007-2013 under REA grant agreement 290110, SONORUS "Urban Sound Planner".

References

[1] J. S. Hesthaven, S. Gottlieb, and D. Gottlieb, Spectral Methods for Time-Dependent Problems. Cambridge: Cambridge University Press, 2007.

[2] M. Hornikx, R. Waxler, and J. Forssén, "The extended Fourier pseudospectral time-domain method for atmospheric sound propagation.," J. Acoust. Soc. Am., vol. 128, no. 4, pp. 1632–46, Oct. 2010.

[3] V. E. Ostashev, D. K. Wilson, L. Liu, D. F. Aldridge, N. P. Symons, and D. Marlin, "Equations for finite-difference, time-domain simulation of sound propagation in moving inhomogeneous media and numerical implementation," J. Acoust. Soc. Am., vol. 117, no. 2, p. 503, Jan. 2005.

[4] Q. H. Liu, "The PSTD algorithm: A time-domain method requiring only two cells per wavelength," Microw. Opt. Technol. Lett., vol. 15, no. 3, pp. 158–165, Jun. 1997.

[5] Q. H. Liu, "The pseudospectral time-domain (PSTD) algorithm for acoustic waves in absorptive media," IEEE Trans. Ultrason. Ferroelectr. Freq. Control, vol. 45, no. 4, pp. 1044–55, Jan. 1998.

[6] C. Spa, J. Escolano, and A. Garriga, "Semi–empirical boundary conditions for the linearized acoustic Euler equations using Pseudo–Spectral Time-Domain methods," Appl. Acoust., vol. 72, no. 4, pp. 226–230, Mar. 2011.

[7] M. Hornikx, W. De Roeck, and W. Desmet, "A multi-domain Fourier pseudospectral time-domain method for the linearized Euler equations," J. Comput. Phys., vol. 231, no. 14, pp. 4759–4774, May 2012.

[8] J. Utzmann, T. Schwartzkopff, M. Dumbser, and C.-D. Munz, "Heterogeneous Domain Decomposition for Numerical Aeroacoustics," in Multifield Problems in Solid and Fluid Mechanics SE - 13, vol. 28, R. Helmig, A. Mielke, and B. Wohlmuth, Eds. Springer Berlin Heidelberg, 2006, pp. 429–459.

[9] J. S. Hesthaven and T. Warburton, "Nodal discontinuous Galerkin methods: Algorithms, analysis and applications." Springer, 2008.

[10] J. . Williamson, "Low-storage Runge-Kutta schemes," J. Comput. Phys., vol. 35, no. 1, pp. 48–56, Mar. 1980.

[11] T. Toulorge and W. Desmet, "Optimal Runge–Kutta schemes for discontinuous Galerkin space discretizations applied to wave propagation problems," J. Comput. Phys., vol. 231, no. 4, pp. 2067–2091, Feb. 2012.

[12] Y. Reymen, M. Baelmans, and W. Desmet, "Efficient Implementation of Tam and Auriault's Time-Domain Impedance Boundary Condition," AIAA J., vol. 46, no. 9, pp. 2368–2376, Sep. 2008.

[13] Y. Reymen, W. De Roeck, G. Rubio, M. Baelmans, and W. Desmet, "A 3D Discontinuous Galerkin Method for Aeroacoustic Propagation," International Institute of Acoustics and Vibration Paper 387, July 2005.

[14] C. Bogey and C. Bailly, "A family of low dispersive and low dissipative explicit schemes for flow and noise computations," J. Comput. Phys., vol. 194, no. 1, pp. 194–214, Feb. 2004.

[15] M. H. Carpenter and C. A. Kennedy, "Fourth–order 2N-storage Runge–Kutta schemes," Technical Memorandum NASA–TM-109112, NASA Langley Research Center, Jun. 1994.